

IRIS A_{per}TO



UNIVERSITÀ
DEGLI STUDI
DI TORINO

This is the author's final version of the contribution published as:

Marucco, Arianna; Pellegrino, Francesco; Oliaro-Bosso, Simonetta; Maurino, Valter; Martra, Gianmario; Fenoglio, Ivana

Indoor illumination: A possible pitfall in toxicological assessment of photo-active nanomaterials

in Journal of Photochemistry and Photobiology A: Chemistry, 2018, January, 350, 23-31, Available online 18 September 2017.

The publisher's version is available at:

10.1016/j.jphotochem.2017.08.072

When citing, please refer to the published version.

Link to this full text:

<http://hdl.handle.net/2318/317106>

This full text was downloaded from iris-Aperto: <https://iris.unito.it/>

Indoor illumination: a possible pitfall in toxicological assessment of photo-active nanomaterials

Arianna Marucco^{a,b}, Francesco Pellegrino^a, Simonetta Oliaro-Bosso^c, Valter Maurino^a, Gianmario Martra^{a,b}, Ivana Fenoglio^{a,b*}

^a *Department of Chemistry, University of Torino, via P. Giuria 7, 10125 Torino, Italy.*

^b *NIS – Nanostructured Interfaces and Surfaces and ‘G. Scansetti’ Interdepartmental Centre for Studies on Asbestos and other Toxic Particulate, University of Torino, Italy.*

^c *Department of Drug Science and Technology, via P. Giuria 7, 10125 Torino, University of Torino. Italy.*

** corresponding author: Ivana Fenoglio, Department of Chemistry, University of Torino, via P. Giuria 7, 10125 Torino, Italy. e.mail ivana.fenoglio@unito.it. Phone +39 11 6707506.*

Abstract

Standardization of the experimental protocols used in the hazard assessment of nanomaterials (NMs) is strongly required to reduce inconsistency among data deriving by different laboratories. The parameters that are known to modify the toxic response of cells to NMs are in fact higher than for soluble toxicants. Among them illumination, that may induce activation of some semiconducting NMs, has been poorly investigated.

The present study, conducted within the FP7 EU project SETNanoMetro, has been designed to assess the effect of indoor illumination on the oxidative potential and dispersion degree of nano-TiO₂. The generation of Reactive Oxygen Species (ROS) by four nanometric anatase or rutile-

25 anatase TiO₂ specimens under ordinary laboratory illumination has been evaluated by means of
26 Electronic Paramagnetic Resonance (EPR) spectroscopy, while their ability to damage DNA
27 has been measured by agarose gel electrophoresis using plasmid DNA as model. The effect of
28 illumination on nanoparticles dispersion has been evaluated by Dynamic Light Scattering
29 (DLS). The results show the occurrence of photo-activation of TiO₂ under indoor illumination
30 that leads to the generation of ROS and slight plasmid DNA damage. Furthermore, significant
31 differences in the amount of ROS generated were found for small variation of the intensity of
32 the illumination. A small effect on the size distribution of TiO₂ agglomerates in water was
33 observed.

34 The present findings suggest that illumination should be included among the parameters that
35 have to be controlled during toxicological assessment of photo-active nanomaterials.

37 **Keywords**

38 Nanomaterials; reactive oxygen species; particle dispersion; toxicological testing; illumination.

40 **1. Introduction**

41 The knowledge of the hazard is a fundamental pre-requisite to reduce the risk associated to the
42 exposure to chemicals. The current European regulation (REACH), places responsibility on
43 industry to provide safety information on the substances. As consequence, test method
44 standardization for hazard assessment is strongly needed [1, 2]. In the case of nanomaterials
45 (NMs) standardization is a particularly relevant issue. Numerous specific and non-specific
46 factors have been shown to influence the results of toxicological testing [3], such as: i) the
47 degree of dispersion of the NM, that varies depending upon the media used [4,5,6], ii) the real
48 dose, that, oppositely to molecular substances may not correspond to the nominal one [7,8], iii)
49 the presence of contaminants in the materials like bacterial lipopolysaccharides (LPS) [9] or
50 metal ions [10] iv) the occurrence of artefacts due to adsorption of reagents or intrinsic

51 absorbance/fluorescence of the material [3,11,12]. Much less explored is the effect of
52 illumination during the preparation of samples and NM exposure in toxicological testing.
53 Except in the case in which a specific illumination is necessary due to the kind of endpoint
54 evaluated, incubation of cells in *in vitro* tests is performed in the dark. On the other hand, the
55 preparation of the NMs and the administration to cells is performed in laboratories illuminated
56 by artificial or natural light. During these steps, photo-activation of semiconductors materials
57 like ZnO, CeO₂, NiO or TiO₂ may occur since indoor natural illumination and some artificial
58 light (e.g. halogen lamps) contains UV radiation.

59 Among them titanium dioxide (TiO₂) and TiO₂-based materials are the most widespread NMs
60 [13,14], being used for several purposes, e.g. as UV blockers in sunscreens and plastics [15,
61 16]. TiO₂ is a powerful photo-catalyst. When illuminated with UV light it generates at its
62 surface a high amount of reactive species, a property that finds application in several fields, like
63 in water and air remediation [17] or in the production of self-cleaning coatings and textiles [18].
64 The adsorption of photons with energies higher or equal to the TiO₂ band gap (>3.2 eV for
65 anatase) results in electrons to be excited in the conduction band (e⁻_{CB}) leading to the formation
66 of a positive hole in the valence band (h⁺_{VB}). These charge carriers can recombine each other
67 or migrate at the surface where they react with electron donors or acceptors that diffuse close
68 to the surface [19]. For example, by reacting with water and oxygen, hydroxyl radicals (HO[•]),
69 superoxide radicals (O₂^{•-}), singlet oxygen (¹O₂), hydroperoxyl radicals ([•]OOH) and hydrogen
70 peroxide (H₂O₂) are formed. The generation of such oxygenated radicals and molecules,
71 commonly called Reactive Oxygen Species (ROS), affects the ability of TiO₂ to interact with
72 cells by increasing its oxidative potential, i.e. the ability to induce an oxidative burst [20, 21].
73 The role of particle-derived ROS in the in the photo-toxicity of TiO₂ is well established [22,
74 23]. On the other hand, the toxicity of non-illuminated TiO₂ is not expected to be related to
75 them [24]. Nevertheless, several studies performed in the absence of specific illumination
76 reported TiO₂-induced effects related to the occurrence of oxidative burst [25, 26]. Whether it

77 is a consequence of ROS generated by light-activated TiO₂ or of cell-derived ROS is not clear
78 since in most of the studies the illumination condition used during NMs handling is not
79 described.

80 Another well-known property of TiO₂ is the superhydrophilicity: under irradiation with UV
81 light the abundance of hydrophilic groups at the surface of TiO₂ (Ti-OH) increases, an effect
82 that is reversed in the dark [27]. Superhydrophilicity may affect the agglomeration degree of
83 TiO₂ suspensions in water. In fact, particle agglomeration may occur in colloidal suspensions
84 when particles exhibit a low osmotic repulsion. In this case attractive van der Waals forces and
85 entropy driven surface dehydration prevail leading to agglomeration [28]. This largely depends
86 on the thickness of the Stern layer around particles [29] that in turn depends upon particles
87 surface chemistry, in particular the abundance and type of charged groups.

88 Indeed, a light-induced disaggregation of TiO₂ nanoparticles under UV light was previously
89 reported [30].

90 The present study is aimed to assess the effect of indoor illumination on the oxidative potential
91 and dispersion degree of nano-TiO₂. Four samples of fully characterized nano-TiO₂ in the
92 anatase or anatase-rutile forms, the most photo-active ones, has been selected and analyzed for
93 their ability to generate ROS in different illumination conditions by using a set of EPR-based
94 tests previously proposed as integrated protocol for the assessment of biological-relevant photo-
95 activity of TiO₂ [31]. The ability to damage DNA was also tested. Finally, the effect on the NM
96 dispersion, evaluated by means of Dynamic Light Scattering (DLS) analysis was investigated.

97

98 **2. Methods**

99 **2.1 TiO₂ samples.** Four types of titania NMs were considered, three commercial materials (i.e.
100 P25 by Evonik Industries, Germany; SX001 by Solaronix, Swizerland; and PC105 by Cristal,
101 Saudi Arabia) and one lab-made TiO₂ prepared via hydrothermal synthesis, and then coded as
102 UT001. Details of preparation, structural and morphological characterization of the specimens

103 are in ref. [32]. In brief, UT001 was obtained by forced hydrolysis of an aqueous solution of
104 $\text{Ti}(\text{TeoaH})_2$ complex (Teoa = triethanolamine; initial pH 10), carried out by hydrothermal
105 treatment at 453 K for 90 h. Before the use, each material was suspended in water and then
106 processed according to the following procedure in order to remove organic and inorganic
107 impurities adsorbed onto TiO_2 NPs: i) dialysis against ultrapure water (MilliQ, Millipore) using
108 a Spectra/Por dialysis membrane tubing (MWCO 8-12 kD or MWCO 12-14 kD); final pH of
109 the permeated liquid in the 5-6 range, Cl^- and $\text{SO}_4^{2-} < 1$ ppm (by ion chromatography); ii) freeze-
110 drying; iii) re-suspension in milli-Q water; iv) irradiation for 48 hours of the suspension in
111 contact with air, added of 10 ml of H_2O_2 (30%), under UV light using a medium pressure
112 mercury lamp (emission max at 360 nm), ca. 50 W/m^2 in the range 290-400 nm; followed by
113 dialysis and free-drying as steps i) and ii). Step iv) ensures a complete photo-degradation of
114 organic impurities adsorbed onto TiO_2 NPs that can change their surface properties and
115 reactivity of TiO_2 . H_2O_2 is used as electron scavenger to speed up impurities degradation.

116 **2.2 Surface Area Measurements.** The specific surface area (SSA_{BET}) of the powders was
117 measured by adsorption of N_2 at 77 K, applying the BET model for the analysis of results.

118 **2.3 X-ray diffraction (XRD).** X-ray diffraction (XRD) pattern of the powders were recorded
119 with an Analytical X'Pert Pro equipped with an X'Celerator detector powder diffractometer
120 using Cu K α radiation generated at 40 kV and 40 mA. The instrument was configured with $1/2^\circ$
121 divergence and receiving slits. A quartz sample holder was used. The 2θ range was from 20° to
122 80° with a step size ($^\circ 2\theta$) of 0.05 and a counting time of 3 s.

123 **2.4 Morphological Characterization.** TEM images were obtained with a Jeol 3010
124 instrument, operated at 300 kV. For the observation, powders were contacted in dry form with
125 standard Cu grids coated with a lacey carbon film, and then introduced in the microscope. To
126 evaluate the presence of aggregates the samples were also analyzed by Dynamic Light
127 Scattering in 200 mM ammonia solution, in order to maximize the particles electrostatic
128 repulsion, after 30 min sonication and adjusting the concentration depending on the sample

129 characteristics. The Dynamic Light Scattering system used was an ALV (Langen Germany),
130 NIBS model (non invasive backscattering) with fixed scattering angle (173°). Through the
131 Stokes-Einstein equation the hydrodynamic radius r_H of the agglomerates/aggregates were
132 obtained.

133 **2.5 Diffuse reflectance UV-Vis spectroscopy.** The optical behaviour of the powders in the
134 UV-Vis range was investigated by electronic absorption spectroscopy in the diffuse reflectance
135 mode. Spectra were acquired with a Cary 5000 instrument (Varian), equipped with an
136 integrating sphere coated with Spectalon[®], also used as reference. In order to avoid side effects
137 due to differences in particle packing, the powder cell provided by Varian was used, allowing
138 pressing a sample toward the optically pure quartz window constituting the front part of the
139 cell. Proper amounts of powders were used, resulting in layers of ca. 3 mm in thickness, thus
140 reaching the usual condition for correct measurements in the diffuse reflectance mode [33].

141 **2.6 Illumination conditions and light irradiance measurements.**

142 The irradiance in the visible and UV regions was measured with a photo-radiometer (Delta
143 Ohm S. r. L., Padova, Italy) under natural indoor light (windows closed) and artificial
144 illumination (halogen lamp). For the sake of comparison, the irradiance of outdoor natural light
145 was also measured (Table 1). Measurements were made twice a day for one week in the month
146 of September 2016 (Latitude: $45^\circ04'13''$ N
147 Longitude: $7^\circ41'12''$ E). No UVC radiation is expected to be present in solar light and therefore
148 was not measured.

149 Experiments were performed under reduced illumination (shielded light) set up under a hood
150 by shielding the glasses, or under standardized light obtained by using a 500 W Hg/Xe lamp
151 (Oriol Instruments) equipped with an IR water filter to avoid the overheating of the suspensions
152 with or without a 400 nm cut-off filter. The presence of the 400 nm cut-off filter leads a radiation
153 that contains a fraction of UVA/B of intensity intermediate between outdoor and indoor (Table
154 1). Finally experiments were also performed in a dark room with a red led as unique source of

155 light. In this case, each sample was weighted and then kept in the dark room for 24h before
 156 experiments, in order to exclude any activation of the powders.

157

158 **Table 1. Light irradiance at the different illumination conditions**

Light source	Light irradiance (W/m ²)			
	Visible 1050-400 nm	UVA 400-315 nm	UVB 315-280 nm	Total UVA/UVB (calculated)
Hg/Xe lamp	795 ± 73	432 ± 60	836 ± 78	1268
Outdoor	315 ± 119	3.30 ± 1.19	0.28 ± 0.13	3.6
Halogen lamp	7.30 ± 1.50	63.9x10 ⁻³ ± 5.0x10 ⁻³	7.9x10 ⁻³ ± 1.0x10 ⁻³	71.8x10 ⁻³
Natural indoor light	3.30 ± 1.40	25.6x10 ⁻³ ± 8.0x10 ⁻³	0.97 x10 ⁻³ ± 0.3x10 ⁻³	26.6x10 ⁻³
Hg/Xe lamp + filter	560 ± 58	0.164 ± 0.040	3.5 x10 ⁻³ ± 3.0 x10 ⁻³	0.168
Shielded light	0.20 ± 0.06	0.70x10 ⁻³ ± 1.0x10 ⁻³	0.75 x10 ⁻³ ± 0.07	1.4x10 ⁻³
Dark	18.7x10 ⁻³ ± 0.30x10 ⁻³	0.10x10 ⁻³ ± 0.08x10 ⁻³	0.60x10 ⁻³ ± 0.2x10 ⁻³	0.7x10 ⁻³

159

160

161 **2.7 Generation of free radicals and singlet oxygen.** All experiments were performed in
 162 ultrapure MilliQ water (Millipore, Billerica, MA). Amounts of powders corresponding the same
 163 exposed surface area (1.4 m²) calculated on the basis of the SSA_{BET} was used for all
 164 experiments (P25 25mg; PC105 16mg; UT001 30mg; SX001 15mg). The powders were
 165 transferred in a 2.5 ml quartz vial and generation of the different ROS was monitored by adding
 166 the following solutions:

167 1) Total reactivity: 2 ml of a 50μM solution of TEMPONE-H (1-hydroxy-2,2,6,6-tetramethyl-
 168 4-oxo-piperidine, Enzo Life Sciences Inc., Farmingdale, New York, US) in water;

169 2) Oxidative reactivity: 0.5 ml of a solution of DMPO (5,5-Dimethyl-1-pyrroline-N-oxide,
170 Enzo Life Sciences Inc., Farmingdale, New York, US) 88 mM, and sodium formate 1M in
171 phosphate buffer saline (pH 7.5, 0.005M);

172 3) Singlet oxygen generation: 2 ml of a 50 mM solution of 4-oxo-TMP (2,2,6,6-tetramethyl-4-
173 piperidone, Sigma-Aldrich, Saint Louis, Missouri, US) in phosphate buffer saline (pH 7.4,
174 0.01M)

175 The suspensions were exposed to the different illumination conditions for 60 or 40 minutes and
176 the generation of radical species monitored by Electron Spin Resonance (EPR) spectroscopy
177 (Miniscope 100 EPR spectrometer, Magnettech, Berlin, Germany) on aliquots of the
178 suspensions withdrawn with a glass capillary each 10 minutes.

179 Instrument settings: microwave power 7 mW, modulation amplitude 1G, scan time 80s, two
180 scans. The negative controls were, in all experiments, the solutions illuminated in the same
181 conditions as the samples. All experiments were repeated at least three times.

182 The amount of radical generated was evaluated by building a calibration curve with the stable
183 free radicals 4-oxo-TEMPO (or TEMPONE, 4-oxo-2,2,6,6-tetramethylpiperidine-1-oxyl, Enzo
184 Life Sciences Inc., Farmingdale, New York, US) in water in the concentrations range 50 - 0.12
185 μM .

186 **2.8 Generation of hydrogen peroxide.** An amount of powder corresponding to an exposed
187 surface area of 1.4 m^2 was suspended in 2 ml of water in a quartz vial and exposed to the chosen
188 illumination conditions. The powder was removed by filtration (cellulose acetate, $0.20 \mu\text{m}$).

189 The concentration of hydrogen peroxide on the supernatant was evaluated by using the method
190 reported by Mottola et al. [34]. 50 mg of leucocrystal violet (LCV) was dissolved in 80 ml of
191 0.5%(v/v) HCl and diluted to 100 ml with the same solution. A buffer solution was made by
192 mixing equal volume of 2M sodium acetate and 2M of acetic acid and adjusting the pH to 4.5
193 with acetic acid.

194 1 ml of LCV solution was added to a 1 ml of the supernatant. 4 ml of buffer and 0.5 ml of
195 peroxidase (type I from horseradish) (1 mg/mL) was added and the solution diluted to 10 ml
196 with water. The absorbance was measured after 10 minutes at of the sample at 596 nm against
197 a reference prepared in the same manner but with no powder (Kontron Instruments Inc., Everett,
198 MA). The concentration of hydrogen peroxide was determined by building a calibration curve.

199 **2.9 Direct plasmid DNA damage.** Plasmids are convenient model systems to study direct DNA
200 damage because their sizes are well defined, the quantification of their single breaks (SSBs) by
201 gel electrophoresis is relatively easy and accurate, the chemical environment of the DNA can
202 be precisely controlled, and there is no biological repair processes [35]. Here pYES2 plasmid
203 DNA (Invitrogen, Italy) was used as a model. The damage was quantified in terms of single
204 (SSB) and double (DSB) breaks in the DNA strand. Strand breaks were detected by agarose (1
205 %) gel electrophoresis which separates the three forms of DNA molecules, supercoiled DNA
206 (undamaged plasmid); open circular DNA (resulting from single-strand breaks); linear DNA (a
207 product of double-strand breaks). Experiments were performed in a quartz vial with 0.2 mg of
208 powder suspended in 30 μ l of MilliQ water and then vortexed. To this suspension 5 μ l of DNA
209 solution (about 50 ng/ μ l) were added and then exposed for 20 minutes to the different
210 illumination conditions. As control, DNA was exposed to the corresponding illumination
211 condition, for the same time in the absence of any powder in order to exclude a direct damage
212 to this molecule. After the exposure time (20 min) the suspension was centrifuged (15000 g)
213 and the supernatant was used for gel electrophoresis. DNA bands were stained and visualized
214 with ethidium bromide (Promega, Italy).

215 Controls of the different forms of plasmid DNA were obtained by digesting the supercoiled
216 DNA with EcoRI enzyme in the presence or in the absence of ethidium bromide [23].

217 **2.10 Hydrodynamic diameter.** The hydrodynamic diameter was evaluated by dynamic light
218 scattering (DLS) (Zetasizer Nano-ZS, Malvern Instruments, Worcestershire, U.K., detection
219 limits 1 nm–6 μ m) in ultrapure water or in a 0.05 wt% solution of bovine serum albumin (BSA,

220 Sigma-Aldrich, Saint Louis, Missouri, US) by using a dispersion protocol adapted from the EU-
221 FP7 project NanoGenoTox deliverable 3 (<http://www.nanogenotox.eu>). Briefly, a 2.56 mg/ml
222 stock dispersion was prepared by pre-wetting powder in 0.5 vol% ethanol (96% purity)
223 followed by dispersion in 0.05 wt% BSA and sonicated for 35 minutes with a probe sonicator
224 (100 W, 40% amplitude, 20 kHz, 3 mm titania probe, Sonoplus, Bandelin, Berlin, Germany).
225 The time of sonication and the amplitude of the sonicator power were set-up to deliver a pre-
226 determined acoustic power according to the method developed within the EU-FP7 project
227 NANoReg. DLS analysis was started after 10 minutes of incubation in the various illumination
228 conditions. The results are the mean of three independent measurements each consisting in
229 consecutive 10 runs on the same vial.

230

231 **3. Results**

232 **3.1 Physico-chemical characterization of the TiO₂ samples**

233 The XRD patterns of the four selected materials show that all materials are pure anatase, except
 234 for P25 which is a mixture of anatase/rutile (Table 2 and SI).

235

236 **Table 2. Main physico-chemical features of the TiO₂ samples**

	Crystalline phase^a	Impurities	Specific surface area (m²/g)^b	Primary particle size (nm)^c	Hydrodynamic diameter (nm, NH₃ 0.2 M)^d
P25	Anatase 80% Rutile 20%	-	55	30	36
PC105	Anatase >99%	sulphates	86	23	630 (aggregates)
UT001	Anatase >99%	carbonates/ carboxylates	47	33	34
SX001	Anatase	carbonates/ carboxylates	93	19	82 (aggregates)

237 ^a XRD; ^b BET; ^c TEM; ^d DLS

238

239 UT001 exhibits a quite regular bi-pyramidal shaped nanoparticles with regular borders [32]
 240 whereas P25, PC105 [36] and SX001 [37] are characterized by less regular profiles (Figure S1
 241 in SI), in agreement with the presence of a significant fraction of surface terminations different
 242 from {101} previously facets (the most stable ones), as probed by IR spectroscopy of adsorbed
 243 CO [37].

244 The trend exhibited by the specific surface area (SSA) is in qualitative agreement with the size
 245 of primary nanoparticles (the smaller the size, the larger the SSA). Nevertheless, only UT001
 246 and P25 nanoparticles attained a mono-dispersion when suspended in a proper aqueous
 247 medium, whereas even in the best dispersion condition attained the other two TiO₂ powders

248 exhibited hydrodynamic diameters larger than primary particles, indicating they are constituted
249 by agglomerates of nanoparticles, quite huge in size for PC105 [38].

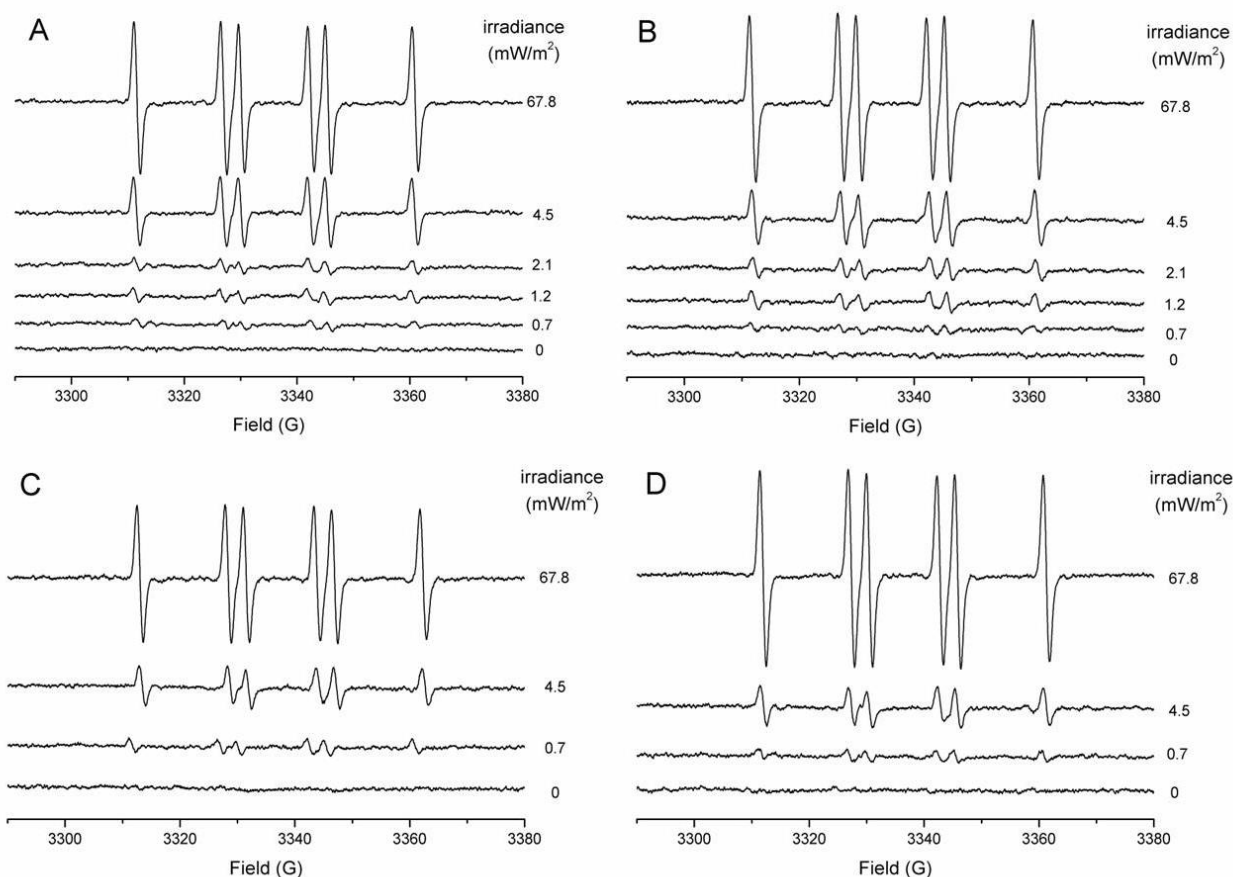
250 All samples appeared, as expected, opaque to UV radiation and transparent to visible light
251 (Figure S2 in SI). The Kubelka-Munk vs. wavelength spectra exhibited the typical absorption
252 edge due to the valence-to-conduction band transition [39]. As expected, the absorption edge
253 of P25 (anatase:rutile \approx 80:20 by weight) is located at longer wavelength with respect the pure
254 anatase materials, because of the narrower inter-band energy gap of rutile [40]. In all cases the
255 onset of the absorption is located in the high energy part of the visible range, due to the coupling
256 of photon absorption with phonon emission, one of the two results of the indirect character of
257 the inter-band transition [41,42]. Nevertheless, an additional localized absorption seems to be
258 present in the visible range of the spectrum of PC105, which could be due to localized charged-
259 transfer absorptions related to the presence on the surface of these TiO₂ nanoparticles of
260 sulphate groups.

261

262 **3.2 Effect of UV radiation intensity of TiO₂ photo-reactivity**

263 Preliminary experiments conducted in normal indoor light unexpectedly showed a significant
264 photo-activation of all powders. However, the amount of radicals generated was highly variable
265 during the day and the seasons, because of the different intensity of the light (Table 1). The
266 activation of the TiO₂ powders was also monitored by gradually shielding the laboratory natural
267 light down to the minimal amount of visible light allowing to operate, and by measuring the
268 reactivity of the powder toward sodium formate at fixed irradiance values .

269



270

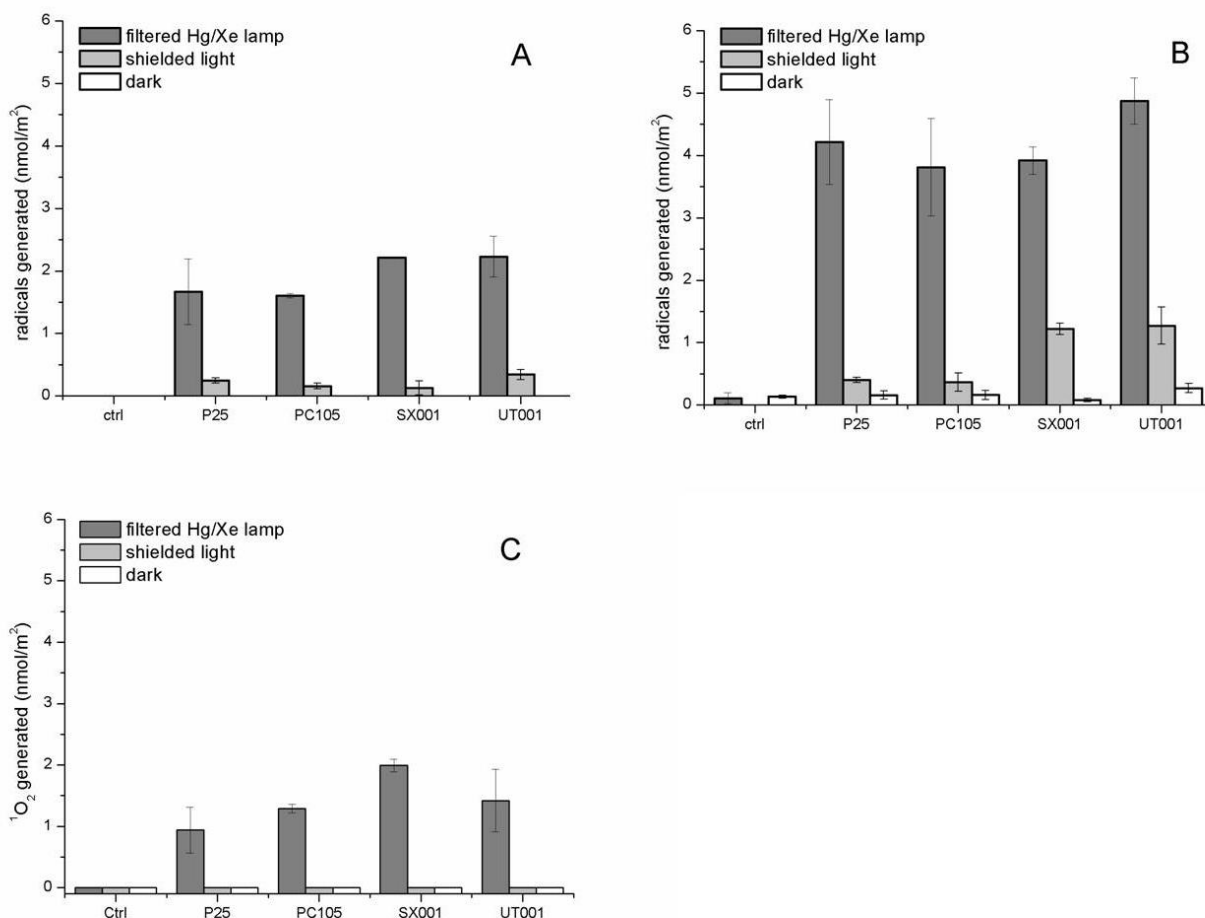
271 **Figure 1. Effect of light intensity on TiO₂ activation.** EPR signals recorded after 60 minutes of
 272 incubation of A) P25; B) UT001; C) PC105; D) SX001 in a buffered solution (PBS, 0.005M, pH 7.5)
 273 containing 1M sodium formate and 88mM DMPO. The irradiance values (UVA) measured during the
 274 experiments are reported on the graphs.
 275

276 The EPR signal intensity (Figure 1), that is proportional to the powder reactivity, was found
 277 largely dependent on the light irradiance for all the samples, despite the differences in the UVA
 278 radiation intensity was very low. At a value of UVA of 0.7 mW/m², correspondent to a total
 279 UVA+UVB 1.4 mW/m² (Table 1) the lowest signal intensity was obtained for all the samples.
 280 This last condition, referred here as "shielded light" can be considered the condition most
 281 widely applicable in practice. For this reason, was chosen for the subsequent experiments.

282 3.3 TiO₂ photo-activation in shielded light

283 A set of tests were used to measure the overall reactivity of TiO₂ that may induce cell damage,
 284 including all ROS species generated by TiO₂ and the oxidative/reductive processes that follow

285 the direct reaction of molecules with the surface charge carriers [43]. This was achieved by
286 EPR spectroscopy using three different probes, sodium formate, the hydroxylamine
287 TEMPONE-H and the piperidone 4-oxo-TMP. Hydrogen peroxide generation was evaluated
288 by a spectrophotometric method as described in the Method Section. The experiments were
289 performed under the shielded light condition described above and the data compared with those
290 obtained by using the filtered Hg/Xe lamp (positive control) or in the dark (negative control) .
291 In Figure 2 the amount of radicals generated in the three illumination conditions, at the last time
292 point considered in the kinetic, are reported. The full kinetics of generation are reported in the
293 SI. A substantial reactivity toward the three probes was observed following irradiation with the
294 filtered Hg/Xe lamp, while no hydrogen peroxide generation was detected in any conditions
295 (not reported). Some differences among samples was observed: UT001 and SX001 were the
296 most reactive toward sodium formate (Figures 2 and S5 in SI), UT001 and P25 appeared the
297 most reactive toward TEMPONE-H (Figures 2 and S4 in SI), while the most active in
298 generating singlet oxygen was SX001 (Figures 2 and S6 in SI). An increase of the amount of
299 ROS generated with time was observed for all samples in all tests (SI).



300

301 **Figure 2. ROS generation by the TiO₂ samples in different illumination conditions.** A) radicals
 302 generated in the presence of sodium formate (oxidative reactivity) ; B) radicals generated in the presence
 303 of TEMPONE-H (total reactivity); C) generation of singlet oxygen. The data are expressed as amount
 304 of radicals generated per unit surface area of the powder, at the last point considered in the kinetic (see
 305 SI). Illumination conditions are indicated in each panel.

306

307 The amount of ROS generated in the shielded light condition was negligible when measured
 308 with sodium formate or 4-oxo-TMP. However, the samples, and in particular UT001 and P25,
 309 was still active toward TEMPONE-H, albeit the amount of ROS generated was one order of
 310 magnitude lower than those generated with the filtered Hg/Xe lamp. Differently to what
 311 previously reported [44], in the dark a negligible reactivity was observed. This was because in
 312 the present case the powders were kept for 24h in the dark, thus suggesting a possible role of
 313 pre-illumination.

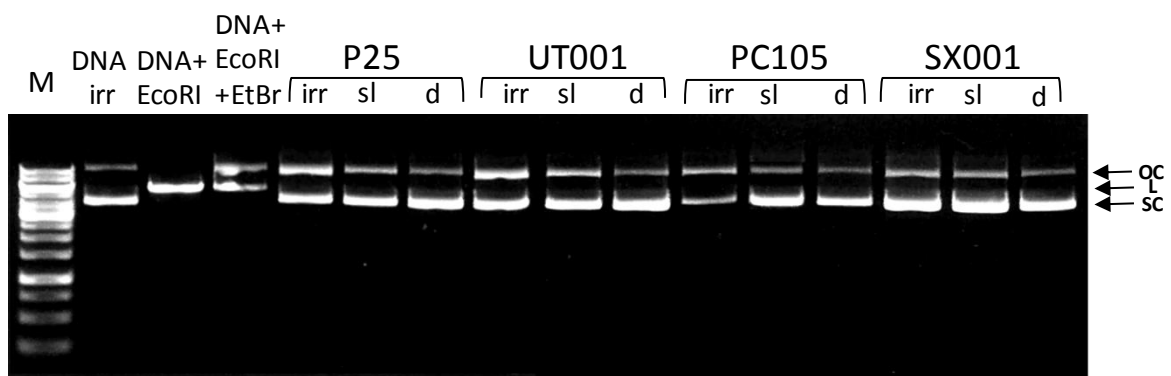
314

315

316 3.4 TiO₂-induced damage to plasmid DNA in shielded light

317 The reactivity was evaluated by incubating the powders with SC-pDNA in the various
318 illumination conditions and by measuring the DNA damage by agarose electrophoresis (Figure
319 3). The induction of DNA strand breaks was evaluated by the conversion of the supercoiled
320 form (SC) to open circular (OC) and linear (L) forms.

321



322

323 **Figure 3. Effect of illumination on TiO₂ -induced damage to double stranded supercoiled plasmid**
324 **DNA.** The plasmid DNA was exposed for 20 min to the TiO₂ samples in different illumination
325 conditions (irr: filtered Hg/Xe lamp, sl: shielded light, d: dark). Damage was evaluated as capability to
326 induce the formation of, open circular DNA (OC) and linear DNA(L) from native supercoiled double
327 stranded DNA (SC). (M) marker; (DNA irr) DNA irradiated by the filtered Hg/Xe lamp without
328 powders; (DNA EcoRI) DNA digested with EcoRI enzyme; (DNA EcoRI+EtBr) DNA digested with
329 EcoRI enzyme + ethidium bromide.

330

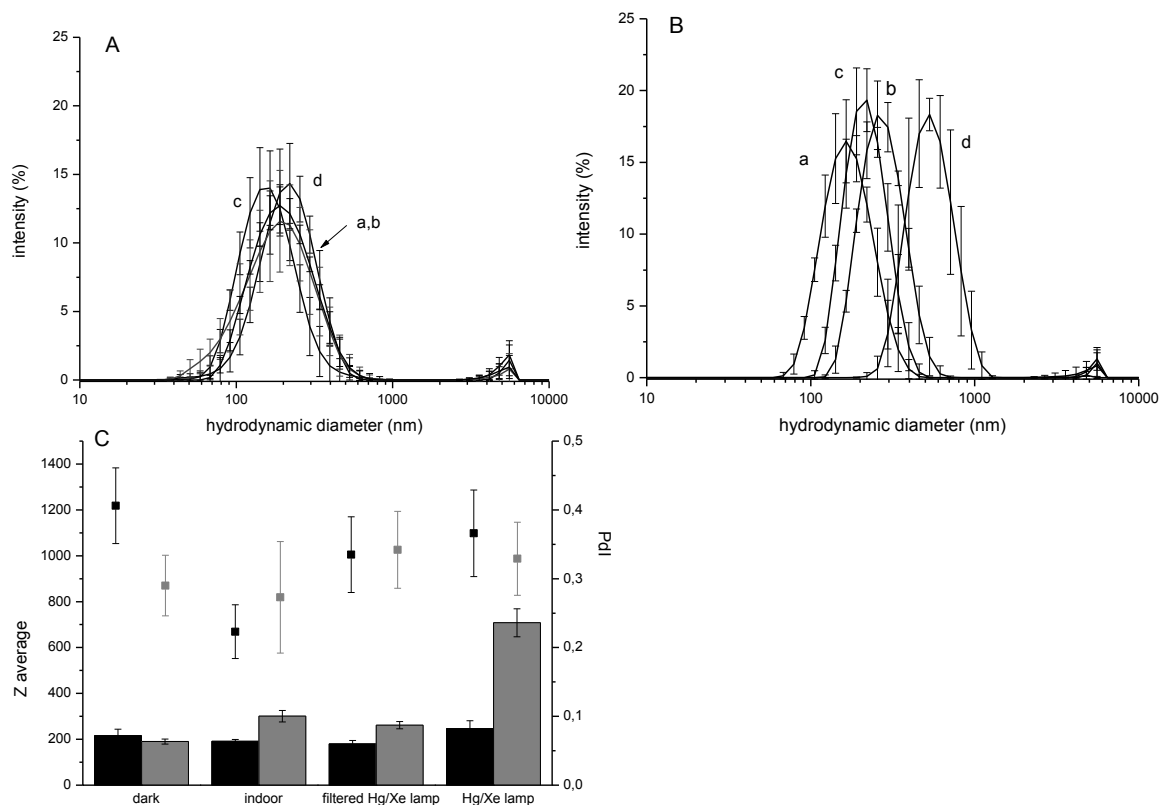
331 As expected, when illuminated with the filtered Hg/Xe lamp, all the TiO₂ samples caused a
332 clear damage to DNA: in fact, an increase in the intensity ratio between the bands correspondent
333 to the open circular (OC) plasmid DNA and supercoiled double stranded DNA (SC) was
334 observed for all samples with respect to plasmid DNA irradiated in absence of powder and the
335 DNA treated with the powders in the dark. This effect is a clearly consequence of a ROS
336 dependent or independent oxidative damage directly induced by activated TiO₂. No bands
337 correspondent to the linear form (L) of DNA was observed. When exposed to shielded light, a

338 very slight increase of the OC/SC intensity band ratio was observed with all samples except
339 than for PC105.

340 3.5 Light-induced aggregation/disaggregation

341 To evaluate the possible effect of illumination on the agglomerate size distribution of TiO₂
342 UT001 was chosen. This sample was the best candidate for DLS analysis since it is composed
343 by particles having a narrow size distribution. The mean hydrodynamic diameter of the powder
344 and the polydispersity index (PDI) were measured in both water and in a 0.05% bovine serum
345 albumin (BSA) solution after sonication following a standardized protocol as described in the
346 method section. Measurements were performed after exposing the suspension for 10 minutes
347 in the dark, indoor light and filtered Hg/Xe lamp. A further condition, i.e. illuminating with the
348 full range of visible, UVA and UVB radiations (Hg/Xe lamp without filter) was also used to
349 induce the highest activation possible of the powders.

350



351

352 **Figure 4. Effect of illumination on TiO₂ dispersions.** Panels A and B: hydrodynamic diameters of
353 UT001 in A) water and B) 0.05% BSA solution, under different illumination conditions: dark (a), indoor
354 light (b), filtered Hg/Xe lamp (c), Hg/Xe lamp (d). Panel C: Z average values (bars) and the
355 polydispersion indexes (PDI) (points) of UT001 in water (black) and in BSA solution (gray).
356

357 In water, the powders appeared organized in agglomerated (Figure 4). No significant variations
358 in mean hydrodynamic diameter were found depending by illumination, except for a moderated
359 shift when the suspension was irradiated with the Hg/Xe lamp. However, a significant decrease
360 of the PDI was observed in all illumination conditions suggesting that disaggregation occurred
361 at some extent. When dispersed in the 0.05% BSA the TiO₂ suspension appeared more
362 uniformly dispersed (lower polydispersion index) in the dark than in water. This was expected
363 since proteins can act as surfactants by adsorbing at the surface and increasing the repulsion
364 among particles. Still, the particles appeared agglomerated, with a small fraction of
365 monodisperse particles. When illuminated, a shift of the mean hydrodynamic diameter toward
366 higher diameters was unexpectedly observed. This effect was particularly relevant after
367 illumination with the UV/vis light. In this conditions, the Z-average value was three time higher
368 than those observed in the dark.

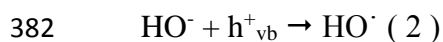
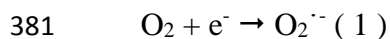
369

370 **4. Discussion**

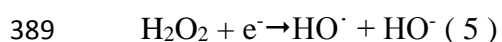
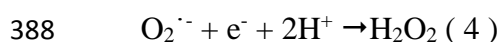
371 The data presented herein demonstrate that, in spite of the very low amount of UV light in
372 normal indoor natural illumination ($15.94 \pm 4.8 \text{ J/m}^2$ during 10 minutes), photo-activation of
373 TiO₂ occurs, leading possible photo-induced effects on cells during toxicological testing. Since
374 photo-activation is largely dependent upon the intensity of UVA/B radiation, illumination may
375 be considered a possible a source of variability of the toxicological data obtained in different
376 laboratories.

377 **4.1 Identification of the ROS generated in shielded indoor illumination.**

378 TiO₂ is able to generate several different ROS. Photo-generated electrons may reduce oxygen
379 to superoxide radicals (equation 1) while holes oxidize water leading to the generation of the
380 highly reactive hydroxyl radicals (equation 2).



383 Hydroxyl and superoxide radicals may further react to generate secondary species that are
384 hydroperoxyl radicals, the conjugated acid of the superoxide anion (equation 3), and hydrogen
385 peroxide (equation 4). Hydrogen peroxide may further react with conduction band electrons
386 generating hydroxyl radicals (equation 5).



390 Singlet oxygen (¹O₂) is also generated by a mechanism still under discussion [45, 46].

391 Formate ions are sensitive probes for the evaluation of the oxidative reactivity of TiO₂ [47],
392 since they are able to react with both photo-generated holes and hydroxyl radicals to form
393 carboxylate radicals, but not with superoxide radicals. Oppositely, TEMPONE-H measures
394 the total reactivity of TiO₂, being able to reacts with all species, included superoxide radicals,
395 forming the stable radical specie TEMPONE.

396 In the shielded light condition used, the reactivity of the powders toward sodium formate was
397 very low (Figure 5A). At the same time no singlet oxygen (Figure 5C) or H₂O₂ generation (data
398 not shown) was observed. On the other hand, small amount of TEMPONE radicals were
399 detected for SX001 and UT001 in the presence of TEMPONE-H (Figure 5B), likely generated
400 following reaction of the probe with superoxide radicals. The ability of TiO₂ to stabilize
401 superoxide radicals by coordination with Ti⁴⁺ ions exposed at the surface [48] may account for
402 their presence in the reaction system. Alternatively, the higher reactivity of TiO₂ toward

403 TEMPONE-H by respect to formate may be due to the scavenging of the photo-generated
404 electrons by the probe that inhibits the recombination of the charge carriers [49].

405 The occurrence of photo-activation suggests the possible capability of the powders to induce
406 oxidative damage also in the presence of very low amount of light. Among the various possible
407 targets of oxidative damage DNA is the most relevant under a toxicological point of view, since
408 it may be related to cell death, mutation or cancer. Nucleic acids are particularly sensible to
409 ROS [50] that may induce nucleosides oxidation, inter-strand cross-links and strand breaks
410 formation [51]. The ROS most involved are hydroxyl radicals and singlet oxygen, while
411 superoxide radicals are known to be inert toward biomolecules [51]. However, they generate
412 other reactive species through reactions 3-5 or in biological environment through Haber-Weiss
413 cycle [52] and therefore it may indirectly induce DNA damage.

414 The tendency of the molecules to get close enough to the surface to react with both short-living
415 ROS species or directly with charge carriers depends upon several factors like diffusion rate
416 and ability to bind to it. For this reason, it is not possible to directly transfer the reactivity of
417 TiO₂ toward the probes used in EPR experiments to biomolecules. Therefore, the powders were
418 further tested for their ability to induce strand breaks to DNA by a direct mechanism (not
419 mediated by cells stimulation) using supercoiled plasmid double-stranded DNA (SC-pDNA) as
420 model (Figure 3). In shielded light, a very small increase in the intensity ratio between the band
421 correspondent to the open circular plasmid DNA and supercoiled double stranded DNA was
422 observed for all samples except than for PC105. However, this effect was low if compared with
423 those observed with the positive control (filtered Hg/Xe lamp), and likely irrelevant in cells,
424 where natural antioxidant systems are present. On the other hand, we cannot exclude the
425 generation of punctual defects like oxidized nucleosides or cross-links. Further experiments
426 will be necessary to evaluate the relevance of the present findings in cells.

427 **4.2 Variability among anatase samples**

428 The analyzed samples are all uncoated and characterized by the anatase form, the most reactive
429 one. However, they exhibit significant differences in physico-chemical features (Table 2) that
430 may reproduce the variability encountered among the TiO₂ NM commercially available.

431 Albeit all samples are characterized by particles having a predominance of exposed {101}
432 facets and exhibiting higher energy terminations, in the case of UT001 facets are quite regular,
433 whilst other high energy surface terminations, i.e. exposing Ti and O sites with a high
434 coordinative unsaturation level, are present on SX001 [37]. Both UT001 and SX001 have
435 carbonate and carboxylate contaminants, mainly in the bulk, while SX001 has sulphate groups
436 as surface contaminants. The samples differ also for the morphology: UT001 and P25 are
437 composed by single particles, PC105 is actually in the form of quite large aggregates while
438 SX001 is constituted by small aggregates of primary particles. Finally, P25 contains also rutile
439 nanoparticles.

440 Focusing on the optical properties of these materials, differences in surface texture and the
441 occurrence of a limited agglomeration seemed do not result in significant difference in the
442 absorption spectra of UT001 and SX001. Conversely, sulphation and large aggregation
443 appeared related to an enhanced absorption of PC105 in the high energy visible range. Finally,
444 as expected, the presence of rutile in P25 resulted in a shift of the inter-band transition edge
445 toward longer wavelength [39].

446 The ability to generate ROS by the four samples examined was quantitatively and qualitatively
447 similar. However, some differences were observed. In particular, UT001 and SX001 appeared
448 overall more reactive on a surface area unit basis by respect to the other two samples, in the test
449 carried out using TEMPONE-H under shielded illumination conditions (Figure 2). Such
450 differences are not due to adsorption in the visible range, since the only samples having a small
451 adsorption out of the UV range is PC105, but likely to the presence in the bulk and at the surface
452 of carbonate/carboxylate species [36].

453 The effect on plasmid DNA was similar for all samples except for PC105 that exhibited a lower
454 reactivity, in agreement with the lower capability to generate ROS. These data suggest that
455 variability in term of photo-activity may be found depending upon small variation in
456 morphological and surface properties that may be further amplified by the different surface area
457 of the TiO₂ samples.

458 **4.3 Effect of illumination on TiO₂ dispersions.**

459 As discussed in the introduction, illumination was previously reported to affect the
460 agglomeration degree of TiO₂ in water [30]. This is a very important issue since the size of
461 agglomerates is known to modulate both the real dose experienced by cells, due to differences
462 in sedimentation rates, and the cell uptake [7]. In the present case, little changes in mean size
463 were observed in all illumination conditions when the powders were dispersed in water (figure
464 4); however the size distribution of aggregates appeared narrower when illuminated than in the
465 dark, as suggested by the lower polydispersion index, indicating that the photo-activation may
466 affect the dispersion degree of TiO₂ powders. On the other hand, when a protein was added to
467 the system, a clear agglomeration was observed at the more extreme illumination conditions.
468 This effect is relevant since it may occur in cell media, where proteins are generally added as
469 nutrients for cells. To elucidate the reasons of this behaviour is out of the scope of this report
470 and will be the object of further investigation. However, we may speculate that the photo-
471 activation induces conformational changes to the absorbed protein that in turn leads to particle
472 agglomeration.

473

474 **5. Conclusions**

475 In conclusion, the data presented herein indicate that the intensity of illumination during sample
476 preparation and exposure is an important parameter in *in vitro* testing of photo-active
477 semiconducting NMs. It therefore has to be controlled and accurately reported. In fact, the lack
478 of this information may limit the inter-laboratory comparability of toxicological data.

479 Albeit operating in a dark room appears to be the best condition during NMs handling, based
480 on our results for pure anatase or anatase-rutile samples a shielded light, correspondent to a
481 maximum of total UV irradiance of 1.4 mW/m^2 , may be suggested to minimize the effects
482 related to the photo-activation of the samples. Cellular studies are in progress to validate this
483 conclusion. Note however, that the present finding apply only to NMs having optical properties
484 similar to TiO_2 , and not to all photo-active NM, like for example the forms of TiO_2 purposely
485 designed to absorb in the visible region by doping or adsorption of dyes.

486

487 **Acknowledgments**

488 This project has received funding from the European Union, Seventh Programme (FP7/2007–
489 2013) under the project “Shape-engineered TiO_2 nanoparticles for metrology of functional
490 properties: setting design rules from material synthesis to nanostructured devices
491 “(SETNanoMetro), grant agreement No. 604577 and under the project “A common European
492 approach to the regulatory testing of nanomaterials” (NANoREG), grant agreement No
493 310584. The Authors are grateful to Alessandra Buffa and Dr. Magda Mocanu that performed
494 the set-up of the illumination conditions and of DLS measurements as part of their post-
495 graduated thesis.

496

497 **References**

- 498 [1] B. Fadeel, V. Kagan, H. Krug, A. Shvedova, M. Svartengren, L. Tran, L. Wiklund, There’s
499 plenty of room at the forum: Potential risks and safety assessment of engineered nanomaterials,
500 *Nanotoxicology*. 1 (2007) 73-84.
- 501 [2] A. Pietroiusti, Health implications of engineered nanomaterials, *Nanoscale*. 4 (2012) 1231-
502 1247.
- 503 [3] V. Stone, H. Johnston, RPF. Schins, Development of in vitro systems for nanotoxicology:
504 methodological considerations, *Crit Rev Toxicol*. 39 (2009) 613–626.

505 [4] Opinion on: Risk Assessment of Products of Nanotechnologies, Scientific Committee on
506 Emerging and Newly Identified Health Risks (SCENIHR), 2009.
507 http://ec.europa.eu/health/scientific_committees/emerging/opinions/scenihhr_opinions_en.htm
508 #nano

509 [5] H. Bouwmeester, I. Lynch, H.J. Marvin, K.A. Dawson, M. Berges, D. Braguer, H.J. Byrne,
510 A. Casey, G. Chambers, M.J. Clift, G. Elia, T.F. Fernandes, L.B. Fjellsbø, P. Hatto, L.
511 Juillerat, C. Klein, W.G. Kreyling, L.C. Nicke, M. Riediker, V. Stone, Minimal analytical
512 characterization of engineered nanomaterials needed for hazard assessment in biological
513 matrices, *Nanotoxicology*. 5 (2011) 1-11.

514 [6] F. Catalano, G. Alberto, P. Ivanchenko, G. Dovbenko, and G. Martra, Effect of silica surface
515 properties on the formation of multilayer or submonolayer protein hard corona: albumin
516 adsorption on pyrolytic and colloidal SiO₂ nanoparticles, *J. Phys. Chem. C*. 119 (2015) 26493-
517 26505.

518 [7] J. Ponti, R. Colognato, H. Rauscher, S. Gioria, F. Broggi, F. Franchini, C. Pascual, G.
519 Giudetti, F. Rossi, Colony forming efficiency and microscopy analysis of multi-wall carbon
520 nanotubes cell interaction, *Toxicol Lett*. 197 (2010) 29-37.

521 [8] D. Lison, G. Vietti, S. van der Brule, Paracelsus in nanotoxicology, *Particle and Fibre*
522 *Toxicology*. 11 (2014) 35.

523 [9] M.G. Bianchi, M. Allegri, A.L. Costa, M. Blosi, D. Gardini, C. Del Pivo, A. Prina-Mello,
524 L. Di Cristo, O. Bussolati, E. Bergamaschi, Titanium dioxide nanoparticles enhance
525 macrophage activation by LPS through a TLR4-dependent intracellular pathway, *Toxicol Res*.
526 4 (2015) 385-398.

527 [10] E. Aldieri, I. Fenoglio, F. Cesano, E. Gazzano, G. Gulino, D. Scarano, A. Attanasio, G.
528 Mazzucco, D. Ghigo, B. Fubini, The role of iron impurities in the toxic effects exerted by short
529 MWCNT in murine alveolar macrophages, *J Toxicol Environ Health Part A*. 76 (2012) 1056-
530 1071.

- 531 [11] F. Schrurs, D. Lison, Focusing the research efforts, *Nature Nanotech.* 7 (2012) 546-548.
- 532 [12] A. Marucco, F. Catalano, I. Fenoglio, F. Turci, G. Martra, F. Fubini, Possible chemical
533 source of discrepancy between in vitro and in vivo tests in nanotoxicology caused by strong
534 adsorption of buffer components, *Chemical research in toxicology.* 28 (2015) 87-91.
- 535 [13] F. Piccinno, F. Gottschalk, S. Seeger, B. Nowack, Industrial production quantities and uses
536 of ten engineered nanomaterials in Europe and in the world, *Nanopart Res.* 14 (2012) 1109-
537 1118.
- 538 [14] OECD, Guidance document 116 on the conduct and design of chronic toxicity
539 and carcinogenicity studies, supporting test guidelines 451,452 and 453. 2nd edition
540 Series on Testing and Assessment No. 116 ENV/JM/MONO (2011)
- 541 [15] Official Journal of the European Union, Regulation (EC) No.1223/2009 of the
542 european parliament and of the council of 30 November 2009 on cosmetic products.
- 543 [16] N. Serpone, D. Dondi, A. Albini, Inorganic and organic UV filters: Their role and efficacy
544 in sunscreens and suncare products, *Inorg Chim Acta.* 360 (2007) 794-802.
- 545 [17] A.G. Agrios, P. Pichat, State of the art and perspectives on materials and applications of
546 photocatalysis over TiO₂, *J appl electrochem.* 35 (2005) 655-663.
- 547 [18] S. Ortelli, M. Blosi, S. Albonetti, A. Vaccari, M. Dodi, A.L. Costa, TiO₂ based nano
548 photocatalysis immobilized on cellulose substrates, *Photoch Photobio A.* 276 (2014) 58-64.
- 549 [19] M. Chiesa, M.C. Paganini, S. Livraghi, E. Giamello, Charge trapping in TiO₂ polymorphs
550 as seen by Electron Paramagnetic Resonance spectroscopy, *Phys. Chem. Chem. Phys.* 15
551 (2013) 9435-9447.
- 552 [20] T. Finkel, Redox-dependent signal transduction, *Febs let.* 476 (2000) 52-54.
- 553 [21] P. Møller, N.R. Jacobsen, J.K. Folkmann, P.H. Danielsen, L. Mikkelsen, J.G.
554 Hemmingsen, L.K. Vesterdal, L. Forchhammer, H. Wallin, S. Loft, Role of oxidative damage
555 in toxicity of particulates, *Free Radical Res.* 44 (2010) 1-46.

556 [22] H. Ma, A. Brennan, S.A. Diamond, Photocatalytic reactive oxygen species production and
557 phototoxicity of titanium dioxide nanoparticles are dependent on the solar ultraviolet radiation
558 spectrum, *Environ Toxicol Chem.* 31 (2012) 2099-2107.

559 [23] I. Fenoglio, J. Ponti, E. Alloa, M. Ghiazza, I. Corazzari, R. Capomaccio, D. Rembges, S.
560 Oliaro-Bosso, F. Rossi , Singlet oxygen plays a key role in the toxicity and DNA damage of
561 nanometric TiO₂ to human keratinocytes, *Nanoscale.* 5 (2013) 6567-6576.

562 [24] S. Dalai, S. Pakrashi, R.S.S. Kumar, N. Chandrasekaran, A. Mukherjee, A comparative
563 cytotoxicity study of TiO₂ nanoparticles under light and dark conditions at low exposure
564 concentrations, *Toxicol Res.* 1 (2012) 116-130.

565 [25] International Agency for research on cancer (IARC): Carbon black, Titanium dioxide and
566 talc. in: *IARC Monographs on the evaluation of carcinogenic risk to humans.* vol 93, Lyon,
567 2010.

568 [26] S.T. Larsen, P. Jackson, S.S. Poulsen, M. Levin, K.A. Jensen, H. Wallin, G.D. Nielsen , I.
569 K. Koponen, Airway irritation, inflammation, and toxicity in mice following inhalation of metal
570 oxide nanoparticles, *Nanotoxicology.* 10 (2016) 1254-1262.

571 [27] S.H. Wang, T.K. Chen, K.K. Rao, M.S. Wong, Nanocolumnar TiO₂ thin films uniquely
572 incorporated with carbon for visible light photocatalysis, *Appl Catal B-Environ.* 76 (2007) 328-
573 334.

574 [28] J. Israelachvili, *Intermolecular and surface surfaces*, second ed., Academic Press, London,
575 1991.

576 [29] D.J. Shaw, *Introduction to Collid and Surface Chemistry*, fourth ed., Butterworth-
577 Heinemann, 1992.

578 [30] S.W. Bennet, D. Zhou, R. Mielke, A. Keller, Photoinduced disaggregation of
579 TiO₂ nanoparticles enables transdermal penetration, *Plos one.* 7 (2012) 1-7.

580 [31] A. Marucco, E. Gazzano, D. Ghigo, E. Enrico, I. Fenoglio, Fibrinogen enhances the
581 inflammatory response of alveolar macrophages to TiO₂, SiO₂ and carbon nanomaterials,
582 *Nanotoxicology*. 10 (2016) 1-9.

583 [32] C. Deiana, M. Minella, G. Tabacchi, V. Maurino, E. Fois, G. Martra, Surface features of
584 TiO₂ nanoparticles: combination modes of adsorbed CO probe the stepping of (101) facets,
585 *Phys Chem Chem Phys*. 15 (2013) 307-315.

586 [33] G. Kortum, *Reflectance Spectroscopy: Principles, Methods, Applications*, Springer -
587 Verlag, New York, 1969

588 [34] H.A. Mottola, B.E. Simpson, G. Gorin, Absorbimetric determination of hydrogen
589 peroxide submicrogram amounts with leuco crystal violet and peroxidase as catalyst, *Anal*
590 *Chem*. 42 (1970) 410-411

591 [35] M.R. Gual, F.M. Milan, A. Deppman, P.R.P. Coelho, Study of DNA damage with a new
592 system for irradiation of samples in a nuclear reactor, *Appl Radiat Isotopes*. 69 (2011) 373-376.

593 [36] C.L. Bianchi, S. Gatto, C. Pirola, A. Naldoni, A. Di Michele, G. Cerrato, V. Crocellà, V.
594 Capucci, Photocatalytic degradation of acetone, acetaldehyde and toluene in gas-phase:
595 Comparison between nano and micro-sized TiO₂, *Appl Catal B-Environ*. 146 (2014) 123-130.

596 [37] C. Deiana, E. Fois, G. Martra, S. Narbey, F. Pellegrino, G. Tabacchi, On the simple
597 complexity of carbon monoxide on oxide surfaces: facet-specific donation and back donation
598 effects revealed on TiO₂ anatase nanoparticles, *Chem Phys Chem*. 17 (2016) 1956–1960.

599 [38] F. Pellegrino, L. Pellutiè, F. Sordello, C. Minero, E. Ortel, V.-D. Hodoroaba, V. Maurino,
600 Influence of agglomeration and aggregation on the photocatalytic activity of TiO₂
601 nanoparticles” *Appl. Catal. B: Environmental*. 216 (2017) 80-87.

602 [39] G. Martra, E. Gianotti, S. Coluccia, The Application of UV - Visible - NIR Spectroscopy
603 to Oxides, in: S.D. Jackson, J.S.J. Hargreaves (Eds.), *Metal Oxide Catalysis*, Wiley-VCH,
604 Weinheim, 2008, pp. 51-94.

- 605 [40] R.I. Bickely, T. Gonzalez-Carreno, J.S. Lees, L. Palmisano, R.J.D. Tilley, A structural
606 investigation of titanium dioxide photocatalysts, *J Solid State Chem.* 92 (1991) 178-190.
- 607 [41] O. Carp, C.L. Huisman, A. Reller, Photoinduced reactivity of titanium dioxide, *Prog Solid*
608 *State Ch.* 32 (2004) 33-177.
- 609 [42] N. Serpone, E. Pelizzetti, *Photocatalysis Fundamentals and Applications*, Wiley
610 Interscience, New York, 1989.
- 611 [43] A. Marucco, F. Turci, L. O'Neill, H.J. Byrne, B. Fubini, I. Fenoglio, Hydroxyl density
612 affects the interaction of fibrinogen with silica nanoparticles at physiological concentration, *J*
613 *Colloid Interf Sci.* 419 (2014) 86-94.
- 614 [44] I. Fenoglio, G. Greco, S. Livraghi, B. Fubini, Non UV-induced radicals interactions at the
615 surface of TiO₂ nanoparticles that may trigger toxic responses, *Chem Eur J.* 15 (2009) 4614-
616 4621.
- 617 [45] T. Daimon, T. Hirakawa, M. Kitazawa, J. Suetake, Y. Nosaka, Formation of singlet
618 molecular oxygen associated with the formation of superoxide radicals in aqueous suspensions
619 of TiO₂ photocatalysts, *Appl Catal A.* 340 (2008) 169–175.
- 620 [46] A. Lipovsky, L. Levitski, Z. Tzitrinovich, A. Gedanken, and R. Lubart, The different
621 behavior of rutile and anatase nanoparticles in forming oxy radicals upon illumination with
622 visible light: an EPR study, *Photochem Photobiol.* 88 (2012) 14-20.
- 623 [47] A. Marucco, E. Carella, I. Fenoglio, A comparative study on the efficacy of different
624 probes to predict the photo-activity of nano-titanium dioxide toward biomolecules, *RSC*
625 *Advances.* 5 (2015) 89559-89568.
- 626 [48] L. Attwood, D.M. Murphy, J.L. Edwards, T.A. Egerton, R.W. Harrison, An EPR study of
627 thermally and photochemically generated oxygen radicals on hydrated and dehydrated TiO₂
628 surfaces, *Res Chem Intermed.* 29 (2003) 449-465.

629 [49] C. Minero, V. Maurino, E. Pelizzetti, Mechanism of the photocatalytic transformation of
630 organic compounds, in: V. Ramamurthy, K.S. Schanze, (Eds.), *Semiconductor Photochemistry*
631 *and Photophysics*, Marcel Dekker, New York, 2003, pp. 211–229.

632 [50] J. Cadet, T. Douki, J.L. Ravanat, Oxidatively generated damage to cellular DNA by UVB
633 and UVA radiation, *Photochem Photobiol.* 91 (2015) 140-155.

634 [51] Cadet J, T. Douki, J.L.Ravanat, Oxidatively generated damage to the guanine moiety of
635 DNA: mechanistic aspects and formation in cells, *Acc Chem Res.* 41 (2008) 1075-1083.

636 [52] J.P. Kehrer, L.O. Klotz, Free radicals and related reactive species as mediators of tissue
637 injury and disease: implications for health, *Crit Rev Toxicol.* 45 (2015) 765-798.

638

639
640
641
642
643
644
645
646
647
648
649
650
651

Supplementary information

652
653
654
655
656
657

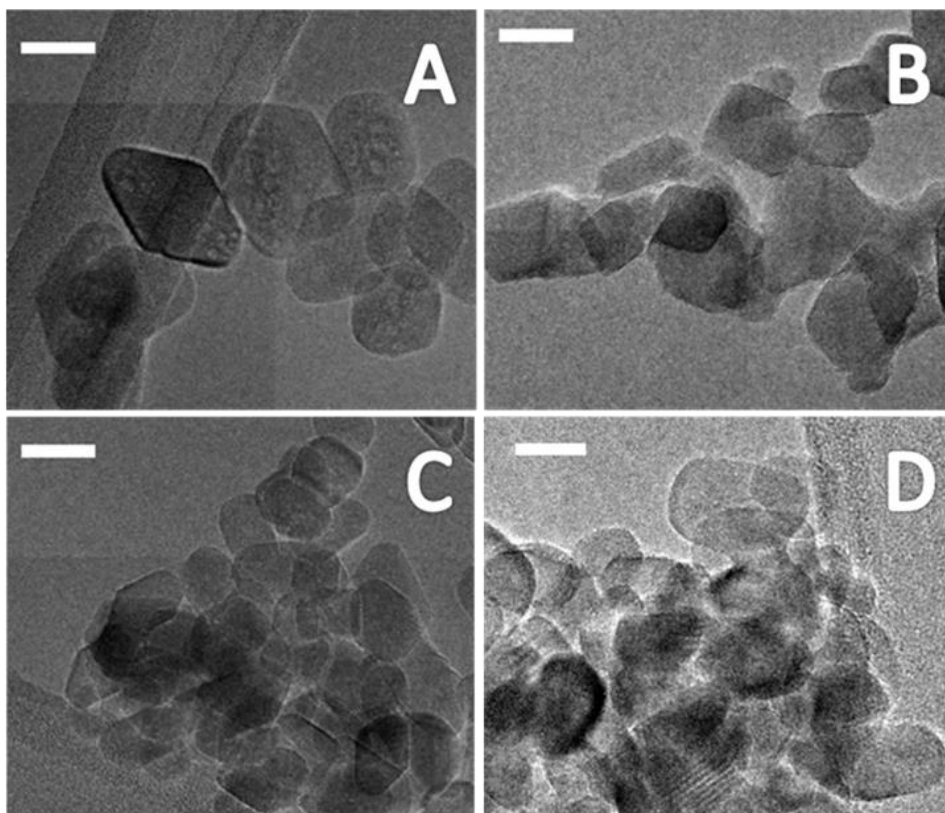
Indoor illumination: a possible pitfall in toxicological assessment of photoactive nanomaterials.

658
659
660
661
662
663
664
665
666
667

Arianna Marucco, Francesco Pellegrino, Simonetta Oliaro-Bosso, Valter Maurino, Gianmario Martra, Ivana Fenoglio*

668
669
670

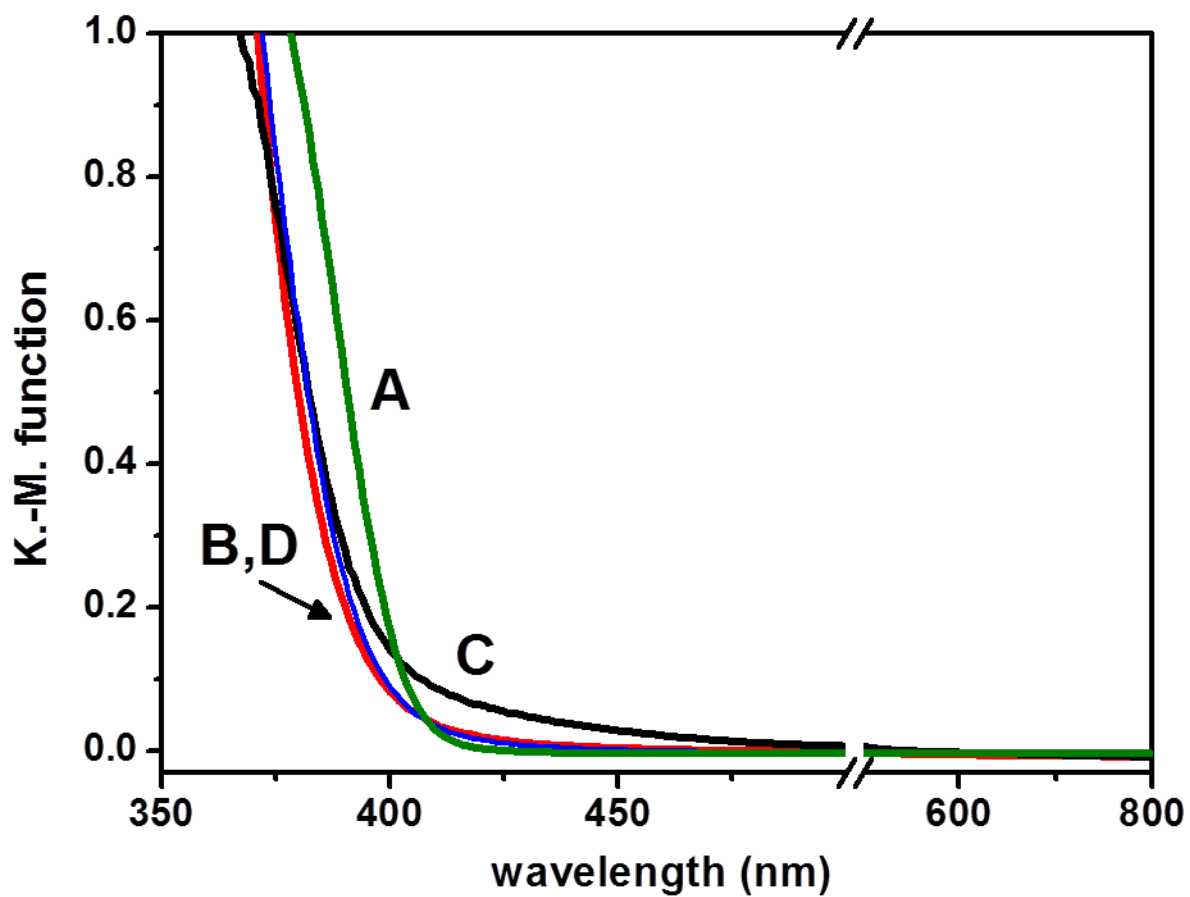
Figure S1. Morphology of the samples. HRTEM micrographs of the four selected materials: (A) UT001, (B) P25, (C) SX001 and (D) PC105. Scale bar in panels = 20 nm.



671
672
673
674
675
676
677
678
679

680
681
682

Figure S2. Adsorption spectra. DR UV-Vis spectra of: A) P25; B) UT001, C) PC105; D) SX001 in air. The Y axis is limited to 1.0, the limit of a correct application of the Kubelka-Munk function (Körtum, 1969).

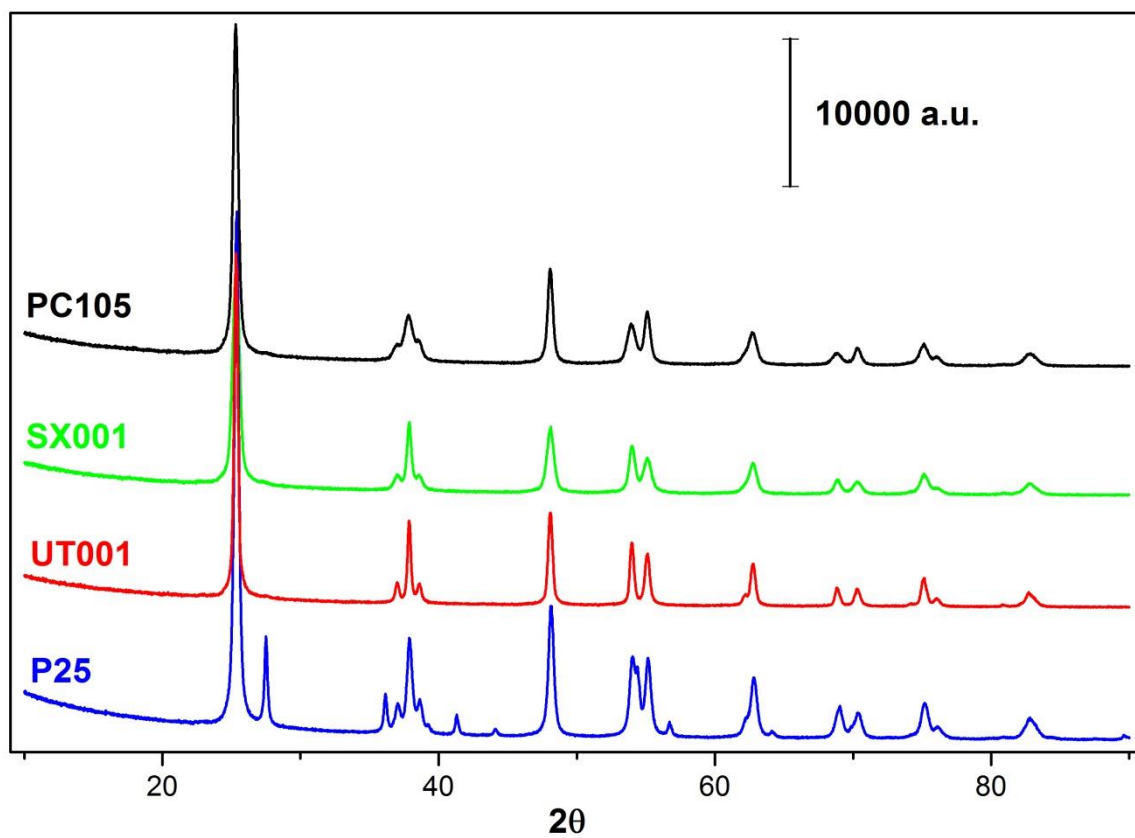


683
684
685
686
687
688
689
690
691
692
693
694
695
696
697
698
699
700
701
702

703

704

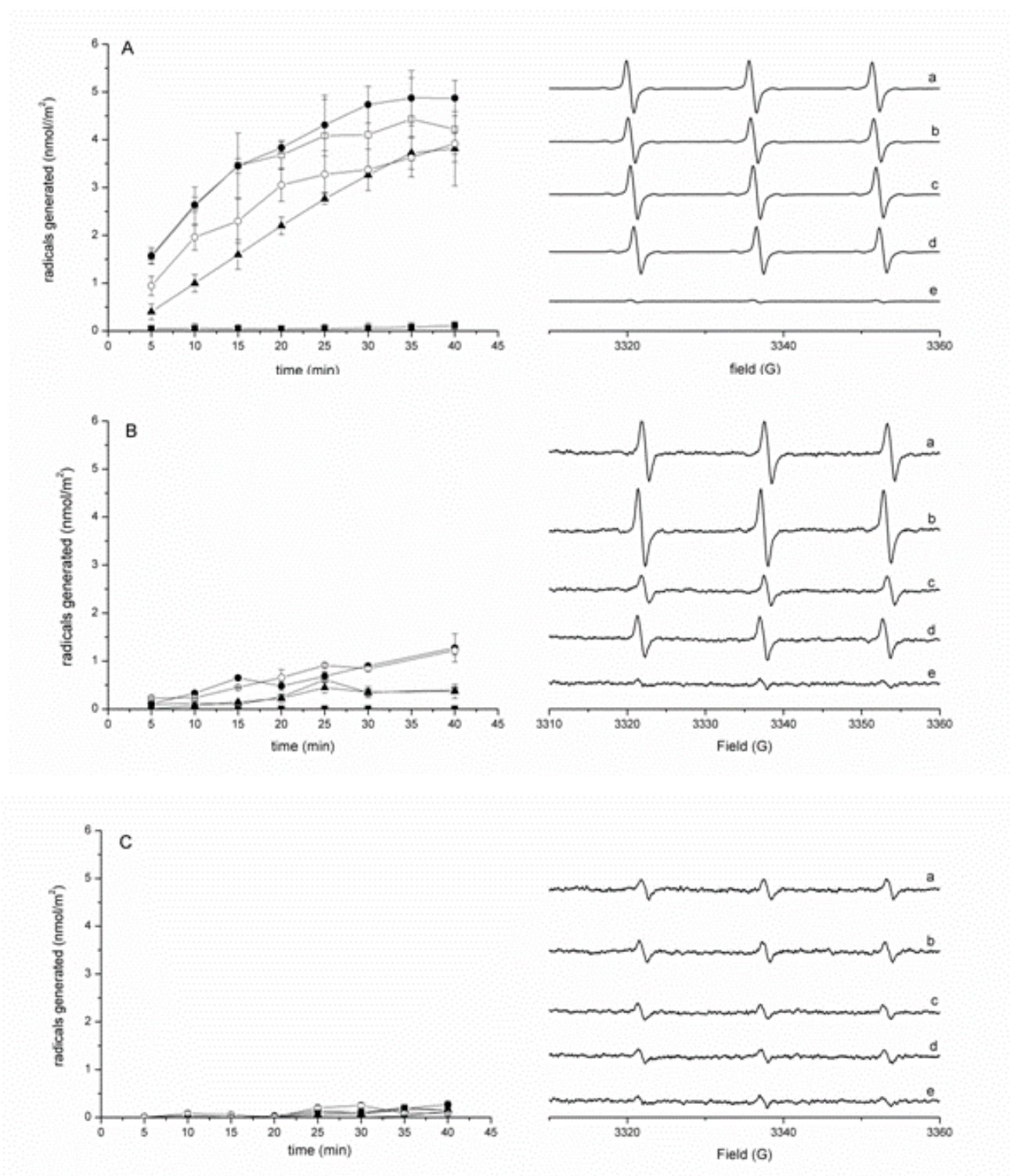
Figure S3. XRD patterns of the samples



705

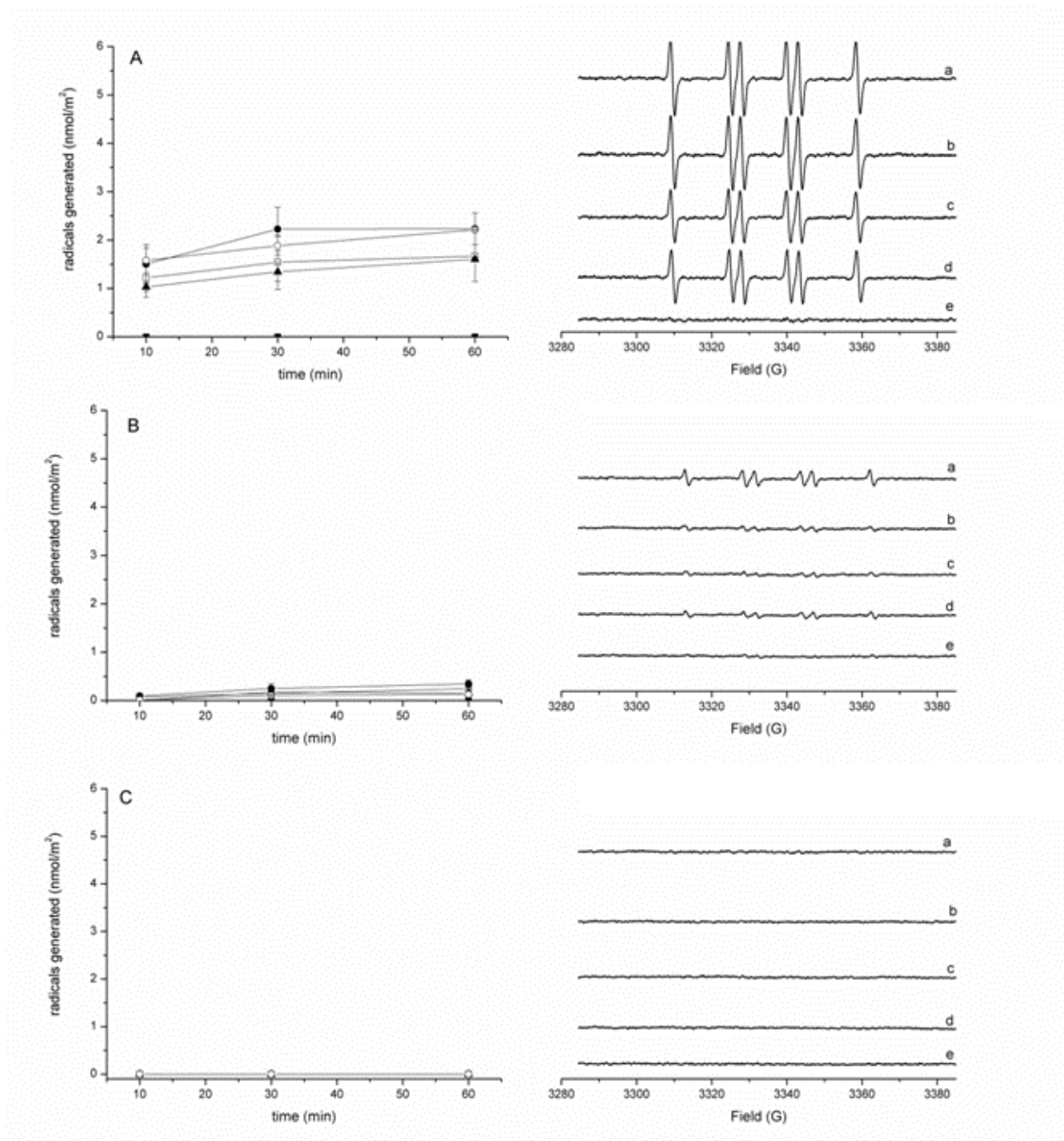
706
707
708
709
710
711
712
713

Figure S4. Reactivity of TiO₂ samples toward TEMPONE-H in different illumination conditions: A) filtered Hg/Xe lamp; B) reduced illumination C) dark. Panels on the left: generation of TEMPONE radicals by the TiO₂ samples (● UT001, ○ SX001, □ P25, ▲ PC105, ■ no powder) when in contact with a solution of TEMPONE-H (50 μM). The data are expressed as amount of radicals generated per unit surface area of the powder. Panels on the right: representative EPR spectra recorded after 40 minutes. (a) UT001, (b) SX001, (c) P25, (d) PC105, (e) no powder. The amount of radicals is proportional to the intensity of the signal.



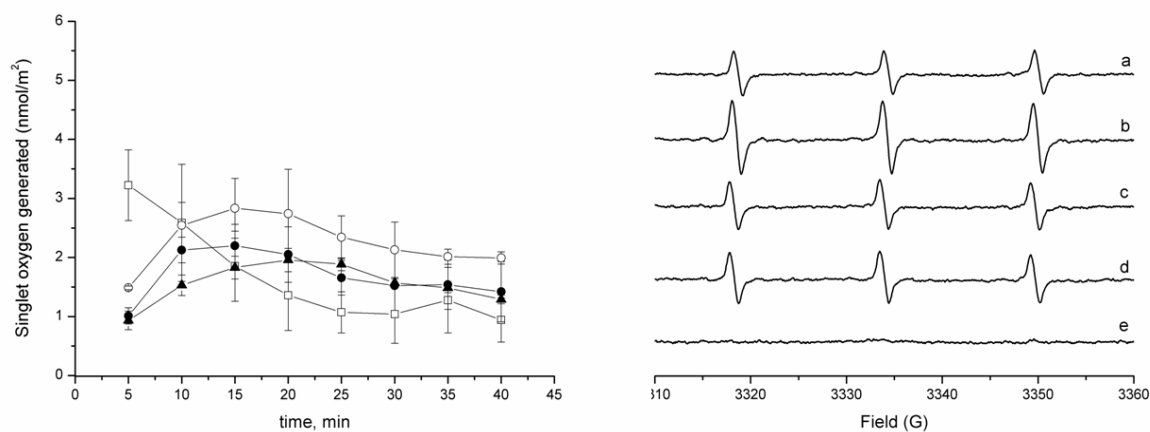
714

715 **Figure S5.Reactivity of TiO₂ samples toward sodium formate in different illumination**
 716 **conditions:** A) filtered Hg/Xe lamp; B) reduced illumination C) dark. Panels on the left:
 717 generation of carboxylate radicals by the TiO₂ samples (● UT001, ○ SX001, □ P25, ▲ PC105, ■
 718 no powder)in contact with a solution (0.005M PBS, pH 7.4, 88mM DMPO) of sodium formate
 719 (1M).The data are expressed as amount of radicals generated per unit surface area of the
 720 powder; Panels on the right: representative spectra recorded after 60 minutes (a) UT001, (b)
 721 SX001, (c) P25, (d) PC105, (e) no powder. The amount of radicals is proportional to the
 722 intensity of the signal.
 723



724
 725
 726

727 **Figure S6. Generation of singlet oxygen by TiO₂ samples.** Panel on the left: amount of
728 TEMPONE radicals generated by the TiO₂ samples (● UT001, ○ SX001, □ P25, ▲ PC105, ■ no
729 powder) in a solution of 4-oxo-TMP (50mM) in phosphate buffer (pH 7.4, 0.01M) when
730 illuminated with the filtered Hg/Xe lamp. Panel on the right: representative spectra recorded
731 after 60 minutes (a) UT001, (b) SX001, (c) P25, (d) PC105, (e) no powder. The amount of
732 radicals is proportional to the intensity of the signal.
733



734
735
736
737
738

739

740

Table S1. Hyperfine splitting constants of the radical species detected

Radical specie	Solvent	Hyperfine constants	splitting
DMPO/CO ₂ ^{·-}	0.005 mM phosphate buffer saline pH 7.4	a _H 15.4 G; a _N 18.5 G	
TEMPONE	water	a _N 15.78 G	
TEMPONE	0.01 mM phosphate buffer saline, pH 7.4	a _N 15.75 G	

741

742